Pan, Y.; and R. N. Horne. "Multivariate Optimization of Field Development Scheduling and Well-Placement Design." *J Petrol Tech* 83–86 (December, 1998).

Ramirez, W. F. *Application of Optimal Control to Enhanced Oil Recovery*. Elsevier, Amsterdam (1998).

Sung, W.; D. Huh; and J. Lee. "Optimization of Pipeline Networks with a Hybrid MCSTCD Networking Model." *SPE Prod Fac* **13**(3): 213–219 (1998).

14

CHEMICAL REACTOR DESIGN AND OPERATION

IN PRACTICE, EVERY chemical reaction carried out on a commercial scale involves the transfer of reactants and products of reaction, and the absorption or evolution of heat. Physical design of the reactor depends on the required structure and dimensions of the reactor, which must take into account the temperature and pressure distribution and the rate of chemical reaction. In this chapter, after describing the methods of formulating optimization problems for reactors and the tools for their solution, we will illustrate the techniques involved for several different processes.

Modeling chemical reactors

Optimization in the design and operation of a reactor focuses on formulating a suitable objective function plus a mathematical description of the reactor; the latter forms a set of constraints. Reactors in chemical engineering are usually, but not always, represented by one or a combination of

1. Algebraic equations
2. Ordinary differential equations
3. Partial differential equations

One extreme of representation of reactor operation is complete mixing in a continuous stirred tank reactor (CSTR); the other extreme is no mixing whatsoever (plug flow). In between are various degrees of mixing within dispersion reactors. Single ideal reactor types can be combined in various configurations to represent intermediate types of mixing as well as nonideal mixing and fluid bypassing.

Ideal reactors can be classified in various ways, but for our purposes the most convenient method uses the mathematical description of the reactor, as listed in Table 14.1. Each of the reactor types in Table 14.1 can be expressed in terms of integral equations, differential equations, or difference equations. Not all real reactors can fit neatly into the classification in Table 14.1, however. The accuracy and precision of the mathematical description rest not only on the character of the mixing and the heat and mass transfer coefficients in the reactor, but also on the validity and analysis of the experimental data used to model the chemical reactions involved.

Other factors that must be considered in the modeling of reactors, factors that influence the number of equations and their degree of nonlinearity but not their form, are

1. The number and nature of the phases present in the reactor (gas, liquid, solid, and combinations thereof)
2. The method of supplying and removing heat (adiabatic, heat exchange mechanism, etc.)
3. The geometric configuration (empty cylinder, packed bed, sphere, etc.)
4. Reaction features (exothermic, endothermic, reversible, irreversible, number of species, parallel, consecutive, chain, selectivity)
5. Stability
6. The catalyst characteristics

Some references for the modeling of chemical reactors include Fogler (1998), Froment and Bischoff (1990), Levenspiel (1998), Missen and colleagues, (1998), and Schmidt (1997).

TABLE 14.1
Classification of reactors

Reactor type	Mathematical description (continuous variables)
Batch [well-mixed (CSTR), closed system]	Ordinary differential equations (unsteady state) Algebraic equation (steady state)
Semibatch [well-mixed (CSTR), open system]	Ordinary differential equations (unsteady state) Algebraic equations (steady state)
CSTRs, individual or in series	Ordinary differential equations (unsteady state) Algebraic equations (steady state)
Plug flow reactor	Partial differential equations in one spatial variable (unsteady state)
	Ordinary differential equations in the spatial variable (steady state)
Dispersion reactor	Partial differential equations (unsteady state and steady state)
	Ordinary differential equations in one spatial variable (steady state)

Abbreviation: CSTR = continuous stirred tank reactor.

Objective functions for reactors

Various questions that lead directly to the formulation of an objective function can be posed concerning reactors. Typical objective functions stated in terms of the adjustable variables are

1. Maximize conversion (yield) per volume with respect to time.
2. Maximize production per batch.
3. Minimize production time for a fixed yield.
4. Minimize total production costs per average production costs with respect to time per fraction conversion.
5. Maximize yield per number of moles of component per concentration with respect to time or operating conditions.
6. Design the optimal temperature sequence with respect to time per reactor length to obtain (a) a given fraction conversion, (b) a maximum rate of reaction, or (c) the minimum residence time.
7. Adjust the temperature profile to specifications (via sum of squares) with respect to the independent variables.
8. Minimize volume of the reactor(s) with respect to certain concentration(s).
9. Change the temperature from T_0 to T_f in minimum time subject to heat transfer rate constraints.
10. Maximize profit with respect to volume.

11. Maximize profit with respect to fraction conversion to get optimal recycle.
12. Optimize profit per volume per yield with respect to boundary per initial conditions in time.
13. Minimize consumption of energy with respect to operating conditions.

In some cases a variable can be independent and in others the same variable can be dependent, but the usual independent variables are pressure, temperature, and flow rate or concentration of a feed. We cannot provide examples for all of these criteria, but have selected a few to show how they mesh with the optimization methods described in earlier chapters and mathematical models listed in Table 14.1.

In considering a reactor by itself, as we do in this chapter, keep in mind that a reactor will no doubt be only one unit in a complete process, and that at least a separator must be included in any economic analysis. Figure 14.1 depicts the relation between the yield or selectivity of a reactor and costs.

All of the various optimization techniques described in previous chapters can be applied to one or more types of reactor models. The reactor model forms a set of constraints so that most optimization problems involving reactors must accommodate steady-state algebraic equations or dynamic differential equations as well as inequality constraints.

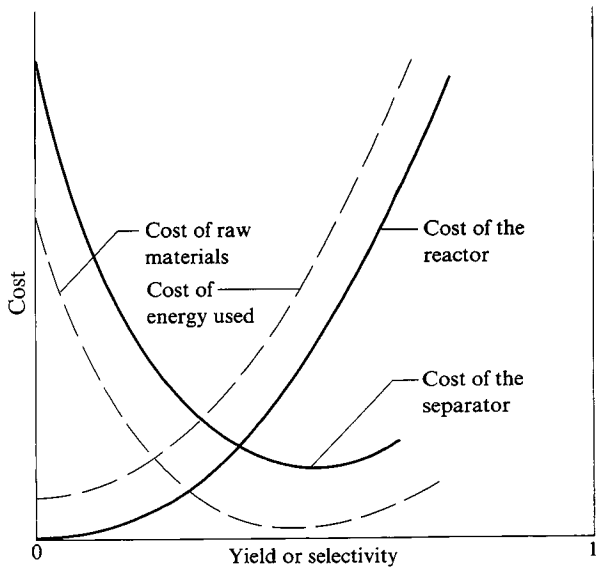

FIGURE 14.1
Costs of energy and raw materials for a reactor as a function of yield and selectivity [Adapted and modified from P. LeGoff, "The Energetic and Economic Optimization of Heterogeneous Reactors," *Chem Eng Sci* **35:** 2089 (1980)].

EXAMPLE 14.1 OPTIMIZATION OF A THERMAL CRACKER VIA LINEAR PROGRAMMING

Reactor systems that can be described by a "yield matrix" are potential candidates for the application of linear programming. In these situations, each reactant is known to produce a certain distribution of products. When multiple reactants are employed, it is desirable to optimize the amounts of each reactant so that the products satisfy flow and demand constraints. Linear programming has become widely adopted in scheduling production in olefin units and catalytic crackers. In this example, we illustrate the use of linear programming to optimize the operation of a thermal cracker sketched in Figure E14.1.

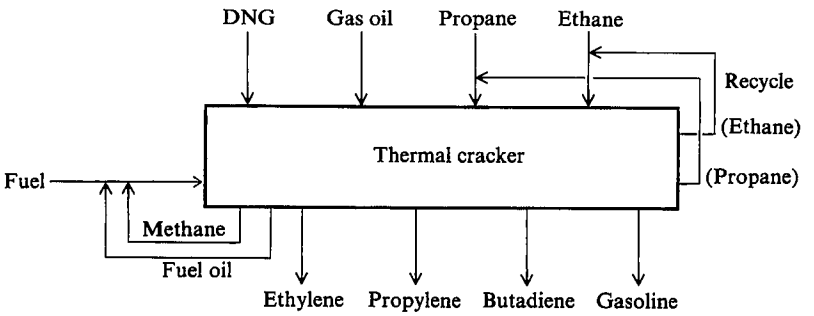

FIGURE E14.1
Flow diagram of thermal cracker.

Table E14.1A shows various feeds and the corresponding product distribution for a thermal cracker that produces olefins. The possible feeds include ethane, propane, debutanized natural gasoline (DNG), and gas oil, some of which may be fed simultaneously. Based on plant data, eight products are produced in varying proportions according to the following matrix. The capacity to run gas feeds through the cracker is 200,000 lb/stream hour (total flow based on an average mixture). Ethane uses the equivalent of 1.1 lb of capacity per pound of ethane; propane 0.9 lb; gas oil 0.9 lb/lb; and DNG 1.0.

TABLE E14.1A
Yield structure: (wt. fraction)

	Feed			
Product	**Ethane**	**Propane**	**Gas oil**	**DNG**
Methane	0.07	0.25	0.10	0.15
Ethane	0.40	0.06	0.04	0.05
Ethylene	0.50	0.35	0.20	0.25
Propane	—	0.10	0.01	0.01
Propylene	0.01	0.15	0.15	0.18
Butadiene	0.01	0.02	0.04	0.05
Gasoline	0.01	0.07	0.25	0.30
Fuel oil	—	—	0.21	0.01

Downstream processing limits exist of 50,000 lb/stream hour on the ethylene and 20,000 lb/stream hour on the propylene. The fuel requirements to run the cracking system for each feedstock type are as follows:

Feedstock type	Fuel requirement (Btu/lb)
Ethane	8364
Propane	5016
Gas oil	3900
DNG	4553

Methane and fuel oil produced by the cracker are recycled as fuel. All the ethane and propane produced is recycled as feed. Heating values are as follows:

Recycled feed	Heat produced (Btu/lb)
Natural gas	21,520
Methane	21,520
Fuel oil	18,000

Because of heat losses and the energy requirements for pyrolysis, the fixed fuel requirement is 20.0×10^6 Btu/stream hour. The price structure on the feeds and products and fuel costs is:

Feeds	Price (¢/lb)
Ethane	6.55
Propane	9.73
Gas oil	12.50
DNG	10.14
Products	**Price (¢/lb)**
Methane	5.38 (fuel value)
Ethylene	17.75
Propylene	13.79
Butadiene	26.64
Gasoline	9.93
Fuel oil	4.50 (fuel value)

Assume an energy (fuel) cost of $\$2.50/10^6$ Btu.

The procedure is to

1. Set up the objective function and constraints to maximize profit while operating within furnace and downstream process equipment constraints. The variables to be optimized are the amounts of the four feeds.
2. Solve using linear programming.
3. Examine the sensitivity of profits to increases in the ethylene production rate.

We define the following variables for the flow rates to and from the furnace (in lb/h):

$$x_1 = \text{fresh ethane feed}$$

$$x_2 = \text{fresh propane feed}$$

x_3 = gas oil feed

x_4 = DNG feed

x_5 = ethane recycle

x_6 = propane recycle

x_7 = fuel added

Assumptions used in formulating the objective function and constraints are

1. 20×10^6 Btu/h fixed fuel requirement (methane) to compensate for the heat loss.
2. All propane and ethane are recycled with the feed, and all methane and fuel oil are recycled as fuel.

A basis of 1 hour is used, and all costs are calculated in cents per hour.

Objective function (profit). In words, the profit f is

$$f = \text{Product value} - \text{Feed cost} - \text{Energy cost}$$

Product value. The value for each product (in cents per pound) is as follows:

Ethylene: $17.75(0.5x_1 + 0.5x_5 + 0.35x_2 + 0.35x_6 + 0.20x_3 + 0.25x_4)$ (a)

Propylene: $13.79(0.01x_1 + 0.01x_5 + 0.15x_2 + 0.15x_6 + 0.15x_3 + 0.18x_4)$ (b)

Butadiene: $26.64(0.01x_1 + 0.01x_5 + 0.02x_2 + 0.02x_6 + 0.04x_3 + 0.05x_4)$ (c)

Gasoline: $9.93(0.01x_1 + 0.01x_5 + 0.07x_2 + 0.07x_6 + 0.25x_3 + 0.30x_4)$ (d)

Total product sales $= 9.39x_1 + 9.51x_2 + 9.17x_3 + 11.23x_4 + 9.39x_5 + 9.51x_6$ (e)

Feed cost.

$$\text{Feed cost } (¢/\text{h}) = 6.55x_1 + 9.73x_2 + 12.50x_3 + 10.14x_4 \qquad (f)$$

Energy cost. The fixed heat loss of 20×10^6 Btu/h can be expressed in terms of methane cost (5.38¢/lb) using a heating value of 21,520 Btu/lb for methane. The fixed heat loss represents a constant cost that is independent of the variables x_i, hence in optimization we can ignore this factor, but in evaluating the final costs this term must be taken into account. The value for x_7 depends on the amount of fuel oil and methane produced in the cracker (x_7 provides for any deficit in products recycled as fuel).

We combine (e) and (f) to get the objective function (¢/h)

$$f = 2.84x_1 - 0.22x_2 - 3.33x_3 + 1.09x_4 + 9.39x_5 + 9.51x_6 \qquad (g)$$

Constraints.

1. Cracker capacity of 200,000 lb/h

$$1.1(x_1 + x_5) + 0.9(x_2 + x_6) + 0.9x_3 + 1.0x_4 \leq 200{,}000 \qquad (h)$$

or

$$1.1x_1 + 0.9x_2 + 0.9x_3 + 1.0x_4 + 1.1x_5 + 0.9x_6 \leq 200{,}000$$

2. Ethylene processing limitation of 100,000 lb/h

$$0.5x_1 + 0.35x_2 + 0.25x_3 + 0.25x_4 + 0.5x_5 + 0.35x_6 \leq 100{,}000 \quad (i)$$

3. Propylene processing limitation of 20,000 lb/h

$$0.01x_1 + 0.15x_2 + 0.15x_3 + 0.18x_4 + 0.01x_5 + 0.15x_6 \leq 20{,}000 \quad (j)$$

4. Ethane recycle

$$x_5 = 0.4x_1 + 0.4x_5 + 0.06x_2 + 0.06x_6 + 0.04x_3 + 0.05x_4 \quad (k)$$

Rearranging, (j) becomes

$$0.4x_1 + 0.06x_2 + 0.04x_3 + 0.05x_4 - 0.6x_5 + 0.06x_6 = 0 \quad (l)$$

5. Propane recycle

$$x_6 = 0.1x_2 + 0.1x_6 + 0.01x_3 + 0.01x_4 \quad (m)$$

Rearranging Equation (m),

$$0.1x_2 + 0.01x_3 + 0.01x_4 - 0.9x_6 = 0 \quad (n)$$

6. Heat constraint
The total fuel heating value (THV) (in Btu/h) is given by

$$\begin{aligned}\text{THV} &= \overbrace{21{,}520x_7}^{\text{fuel}} + \overbrace{21{,}520(0.07x_1 + 0.25x_2 + 0.10x_3 + 0.15x_4 - 0.07x_5 + 0.25x_6)}^{\text{methane from cracker}} \\ &\quad + \overbrace{18{,}000(0.21x_3 + 0.01x_4)}^{\text{fuel oil from cracker}} \\ &= 1506.4x_1 + 5380x_2 + 5932x_3 + 3408x_4 + 1506.4x_5 + 5380x_6 + 21{,}520x_7 \quad (o)\end{aligned}$$

The required fuel for cracking (Btu/h) is

$$\begin{aligned}&\overbrace{8364(x_1 + x_5)}^{\text{ethane}} + \overbrace{5016(x_2 + x_6)}^{\text{propane}} + \overbrace{3900x_3}^{\text{gas oil}} + \overbrace{4553x_4}^{\text{DNG}} \\ &\quad = 8364x_1 + 5016x_2 + 3900x_3 + 4553x_4 + 8364x_5 + 5016x_6 \quad (p)\end{aligned}$$

Therefore the sum of Equation (p) + 20,000,000 Btu/h is equal to the THV from Equation (o), which gives the constraint

$$\begin{aligned}&-6857.6x_1 + 364x_2 + 2032x_3 - 1145x_4 - 6857.6x_5 + 364x_6 \\ &\qquad + 21{,}520x_7 = 20{,}000{,}000 \quad (q)\end{aligned}$$

Table E14.1B lists the optimal solution of this problem obtained using the Excel Solven (case 1). Note that the maximum amount of ethylene is produced. As the ethylene production constraint is relaxed, the objective function value increases. Once the constraint is raised above 90,909 lb/h, the objective function remains constant.

TABLE E14.1B
Optimal flow rates for cracking furnace for different restrictions on ethylene and propylene production

	Flow rate (lb/h)	
Stream	**Case 1**	**Case 2**
x_1 (ethane feed)	60,000	21,770
x_2 (propane feed)	0	0
x_3 (gas oil feed)	0	0
x_4 (DNG feed)	0	107,600
x_5 (ethane recycle)	40,000	23,600
x_6 (propane recycle)	0	1,195
x_7 (fuel added)	32,800	21,090
Ethylene	50,000	50,000
Propylene	1,000	20,000
Butadiene	1,000	5,857
Gasoline	1,000	32,820
Methane (recycled to fuel)	7,000	19,610
Fuel oil	0	1,076
Objective function (¢/h)	369,560	298,590

Suppose the inequality constraints on ethylene and propylene production were changed to equality constraints (ethylene = 50,000; propylene = 20,000). The optimal solution for these conditions is shown as case 2 in Table E14.1B. This specification forces the use of DNG as well as ethane.

EXAMPLE 14.2 OPTIMAL DESIGN OF AN AMMONIA REACTOR

This example based on the reactor described by Murase et al. (1970) shows one way to mesh the numerical solution of the differential equations in the process model with an optimization code. The reactor, illustrated in Figure E14.2a, is based on the Haber process.

$$N_2 + 3H_2 \rightleftharpoons 2NH_3$$

Figure E14.2b illustrates the suboptimal concentration and temperature profiles experienced. The temperature at which the reaction rate is a maximum decreases as the conversion increases.

Assumptions made in developing the model are

1. The rate expression is valid.
2. Longitudinal heat and mass transfer can be ignored.
3. The gas temperature in the catalytic zone is also the catalyst particle temperature.
4. The heat capacities of the reacting gas and feed gas are constant.
5. The catalytic activity is uniform along the reactor and equal to unity.
6. The pressure drop across the reactor is negligible compared with the total pressure in the system.

The notation and data to be used are listed in Table E14.2.

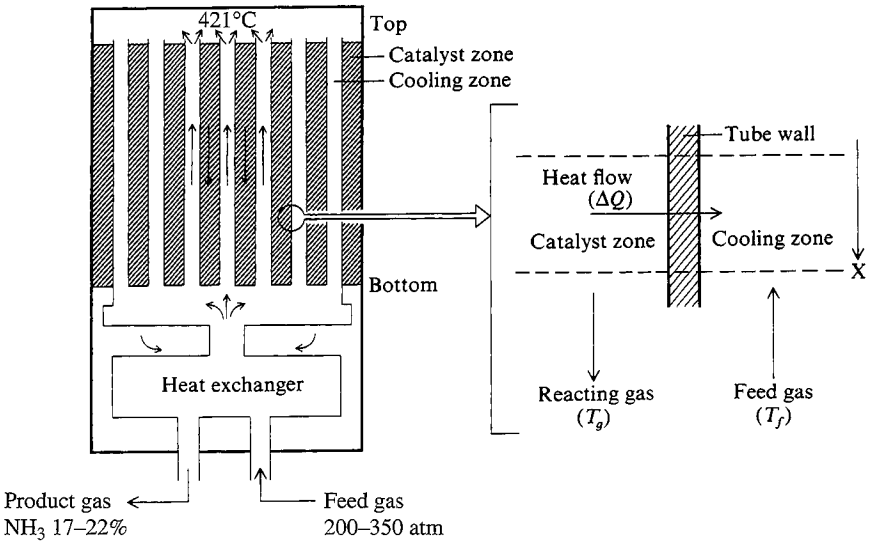

FIGURE E14.2a
Ammonia synthesis reactor. The shaded area contains the catalyst. [Adapted, with permission, from Murase et al., "Optimal Thermal Design of an Auto-thermal Ammonia Synthesis Reactor," *Ind Eng Chem Process Des Dev* **9:** 504 (1970). Copyright, American Chemical Society.]

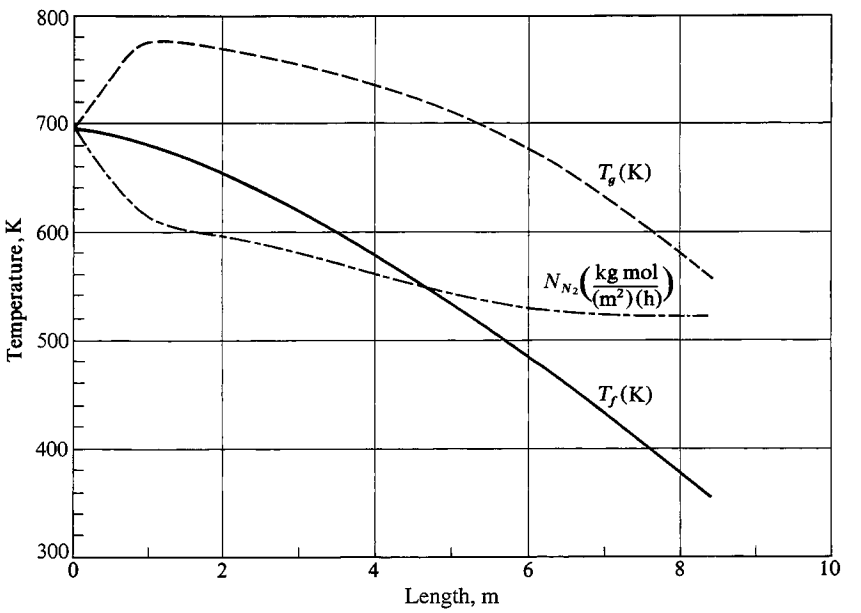

FIGURE E14.2b
Temperature and concentration profiles of the NH_3 synthesis reactor.

TABLE E14.2
Notation and data

Independent and dependent variables	
x	Reactor length, m
N_{N_2}	Mole flow rate of N_2 per area catalyst, kg mol/(m^2)(h)
T_f	Temperature of feed gas, K
T_g	Temperature of reacting gas, K
Parameters	
C_{pf}	Heat capacity of the feed gas = 0.707 kcal/(kg)(K)
C_{pg}	Heat capacity of reacting gas = 0.719 kcal/(kg)(K)
$f(\ )$	Objective function, \$/year
f	Catalyst activity = 1.0
ΔH	Heat of reaction = −26,000 kcal/kg mol N_2
N	Mass flow of component designed by subscript through catalyst zone, kg mol/(m^2)(h)
N_1	Hours of operation per year = 8330
p	Partial pressure of component designated by subscript, psi; reactor pressure is 286 psia
R	Ideal gas constant, 1.987 kcal/(kg mol)(K)
S_1	Surface area of catalyst tubes per unit length of reactor = 10 m
S_2	Cross-sectional area of catalyst zone = 0.78 m^2
T_0	Reference temperature = 421°C (694 K)
U	Overall heat transfer coefficient = 500 kcal/(h)(m^2)(K)
W	Total mass transfer flow rate = 26,400 kg/h

Objective function. The objective function for the reactor optimization is based on the difference between the value of the product gas (heating value and ammonia value) and the value of the feed gas (as a source of heat only) less the amortization of reactor capital costs. Other operating costs are omitted. As shown in Murase et al., the final consolidation of the objective function terms (corrected here) is

$$f(x,N_{N_2},T_f,T_g) = 11.9877 \times 10^6 - 1.710 \times 10^4 N_{N_2} + 704.04T_g - 699.3T_f - [3.4566 \times 10^7 + 2.101 \times 10^9 x]^{1/2} \qquad (a)$$

Equality constraints. Only 1 degree of freedom exists in the problem because there are three constraints; x is designated to be the independent variable.

Energy Balance, Feed Gas

$$\frac{dT_f}{dx} = -\frac{US_1}{WC_{pf}}(T_g - T_f) \qquad (b)$$

Energy Balance, Reacting Gas

$$\frac{dT_g}{dx} = \frac{US_1}{WC_{pg}}(T_g - T_f) + \frac{(-\Delta H)S_2}{WC_{pg}}(f)\left[K_1 \frac{(1.5)p_{N_2}p_{H_2}}{p_{NH_3}} - K_2 \frac{P_{NH_3}}{(1.5)p_{H_2}}\right] \qquad (c)$$

where $K_1 = 1.78954 \times 10^4 \exp(-20{,}800/RT_g)$
$K_2 = 2.5714 \times 10^{16} \exp(-47{,}400/RT_g)$

Mass Balance, N_2

$$\frac{dN_{N_2}}{dx} = -f\left[K_1\frac{(1.5)p_{N_2}p_{H_2}}{p_{NH_3}} - K_2\frac{p_{NH_3}}{(1.5)p_{H_2}}\right] \tag{d}$$

The boundary conditions are

$$T_f(x = L) = 421°C\ (694\ K) \tag{e}$$

$$T_g(x = 0) = 421°C\ (694\ K) \tag{f}$$

$$N_{N_2}(x = 0) = 701.2\ \text{kg mol/(h)(m}^2) \tag{g}$$

For the reaction, in terms of N_{N_2}, the partial pressures are

$$p_{N_2} = 286\left[\frac{N_{N_2}}{1 - 2(N^0_{N_2} - N_{N_2})}\right]$$

$$p_{N_2} = 286\left[\frac{3N_{N_2}}{1 - 2(N^0_{N_2} - N_{N_2})}\right]$$

$$p_{NH_3} = 286\left[\frac{2(N^0_{N_2} - N_{N_2})}{1 - 2(N^0_{N_2} - N_{N_2})}\right]$$

Inequality constraints.

$$0 \le N_{N_2} \le 3220$$

$$400 \le T_f \le 800$$

$$x \ge 0$$

Feed gas composition (mole %).

N_2: 21.75; H_2: 62.25; NH_3: 5; CH_4: 4; Ar: 4

Solution procedure. Because the differential equations must be solved numerically, a two-stage flow of information is needed in the computer program used to solve the problem. Examine Figure E14.2c. The code GRG2 (refer to Chapter 8) was coupled with the differential equation solver LSODE, resulting in the following exit conditions:

	Initial guesses	Optimal solution
N_{N_2}	646 kg mol/(m^2)(h)	625 kg mol/(m^2)(h)
Mole fraction N_2	20.06%	19.4%
T_g	710 K	563 K
T_f	650 K	478 K
x	10.0 m	2.58 m
$f(x)$	8.451×10^5 \$/year	1.288×10^6 \$/year

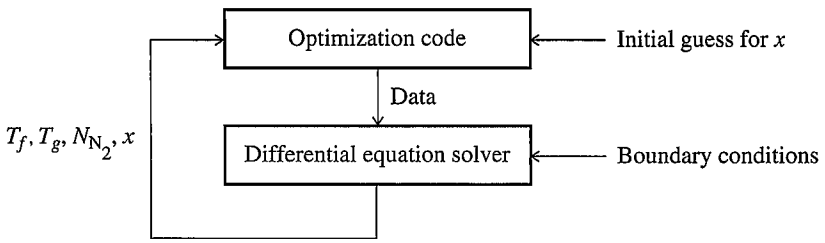

FIGURE E14.2c
Flow diagram for solution procedure, Example 14.2.

In all, 10 one-dimensional searches were carried out, and 54 objective function calls and 111 gradient calls (numerical differences were used) were made by the code.

EXAMPLE 14.3 SOLUTION OF AN ALKYLATION PROCESS BY SEQUENTIAL QUADRATIC PROGRAMMING

A long-standing problem (Sauer et al., 1964) is to determine the optimal operating conditions for the simplified alkylation process shown in Figure E14.3. Sauer and colleagues solved this problem using a form of successive linear programming. We first formulate the problem and then solve it by sequential quadratic programming. The notation to be used is listed in Table E14.3A which includes the units, upper and lower bounds, and the starting values for each x_i (a nonfeasible point). All the bounds represent economic, physical, or performance constraints.

The objective function was defined in terms of alkylate product, or output value minus feed and recycle costs; operating costs were not reflected in the function. The total profit per day, to be maximized, is

$$f(x) = C_1x_4x_7 - C_2x_1 - C_3x_2 - C_4x_3 - C_5x_5 \qquad (a)$$

where C_1 = alkylate product value ($0.063/octane-barrel)
C_2 = olefin feed cost ($5.04/barrel)
C_3 = isobutane recycle costs ($0.035/barrel)
C_4 = acid addition cost ($10.00/per thousand pounds)
C_5 = isobutane makeup cost ($3.36/barrel)

To form the process model, regression analysis was carried out. The alkylate yield x_4 was a function of the olefin feed x_1 and the external isobutane-to-olefin ratio x_8. The relationship determined by nonlinear regression holding the reactor temperatures between 80–90°F and the reactor acid strength by weight percent at 85–93 was

$$x_4 = x_1(1.12 + 0.13167x_8 - 0.00667x_8^2) \qquad (b)$$

The isobutane makeup x_5 was determined by a volumetric reactor balance. The alkylate yield x_4 equals the olefin feed x_1 plus the isobutane makeup x_5 less shrinkage. The volumetric shrinkage can be expressed as 0.22 volume per volume of alkylate yield so that

$$x_4 = x_1 + x_5 - 0.22x_4$$

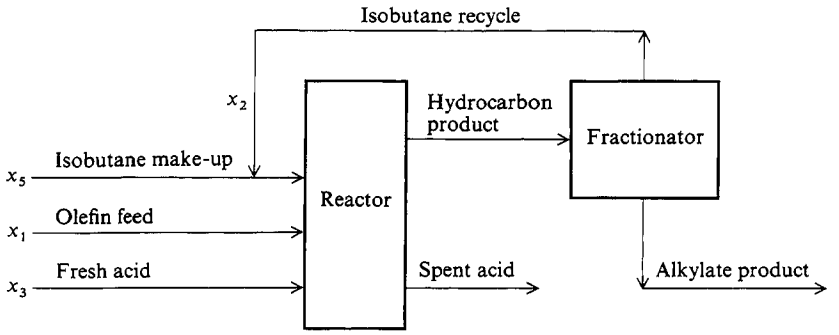

FIGURE E14.3
Alkylation flowsheet.

TABLE E14.3A

Symbol	Variable	Lower * bound	Upper bound	Starting value
x_1	Olefin feed (barrels per day)	0	2,000	1,745
x_2	Isobutane recycle (barrels per day)	0	16,000	12,000
x_3	Acid addition rate (thousands of pounds per day)	0	120	110
x_4	Alkylate yield (barrels per day)	0	5,000	3,048
x_5	Isobutane makeup (barrels per day)	0	2,000	1,974
x_6	Acid strength (weight percent)	85	93	89.2
x_7	Motor octane number	90	95	92.8
x_8	External isobutane-to-olefin ratio	3	12	8
x_9	Acid dilution factor	0.01	4	3.6
x_{10}	F-4 performance number	145	162	145

*Instead of 0, 10^{-6} was used.

or

$$x_5 = 1.22x_4 - x_1 \tag{c}$$

The acid strength by weight percent x_6 could be derived from an equation that expressed the acid addition rate x_3 as a function of the alkylate yield x_4, the acid dilution factor x_9, and the acid strength by weight percent x_6 (the addition acid was assumed to have acid strength of 98%)

$$1000x_3 = \frac{x_4 x_9 x_6}{98 - x_6}$$

or

$$x_6 = \frac{98{,}000x_3}{x_4 x_9 + 1000x_3} \tag{d}$$

The motor octane number x_7 was a function of the external isobutane-to-olefin ratio x_8 and the acid strength by weight percent x_6 (for the same reactor temperatures and acid strengths as for the alkylate yield x_4)

$$x_7 = 86.35 + 1.098x_8 - 0.038x_8^2 + 0.325(x_6 - 89) \qquad (e)$$

The external isobutane-to-olefin ratio x_8 was equal to the sum of the isobutane recycle x_2 and the isobutane makeup x_5 divided by the olefin feed x_1

$$x_8 = \frac{x_2 + x_5}{x_1} \qquad (f)$$

The acid dilution factor x_9 could be expressed as a linear function of the F-4 performance number x_{10}

$$x_9 = 35.82 - 0.222x_{10} \qquad (g)$$

The last dependent variable is the F-4 performance number x_{10}, which was expressed as a linear function of the motor octane number x_7

$$x_{10} = -133 + 3x_7 \qquad (h)$$

The preceding relationships give the dependent variables in terms of the independent variables and the other dependent variables.

Equations (c), (d), and (f) were used as equality constraints. The other relations were modified to form two inequality constraints each, so as to take account of the uncertainty that existed in their formulation. The d_l and d_u values listed in Table E14.3B allow for deviations from the expected values of the associated variables.

Thus, the model has eight inequality constraints in addition to the three equality constraints and the upper and lower bounds on all of the variables.

$$[x_1(1.12 + 0.13167x_8 - 0.00667x_8^2)] - d_{4_l}x_4 \geq 0 \qquad (i)$$

$$-[x_1(1.12 + 0.13167x_8 - 0.00667x_8^2)] + d_{4_u}x_4 \geq 0 \qquad (j)$$

$$[86.35 + 1.098x_8 - 0.038x_8^2 + 0.325(x_6 - 89)] - d_{7_l}x_7 \geq 0 \qquad (k)$$

$$-[86.35 + 1.098x_8 - 0.038x_8^2 + 0.325(x_6 - 89)] + d_{7_l}x_7 \geq 0 \qquad (l)$$

$$[35.82 - 0.222x_{10}] - d_{9_l}x_9 \geq 0 \qquad (m)$$

$$-[35.82 - 0.222x_{10}] + d_{9_u}x_9 \geq 0 \qquad (n)$$

$$[-133 + 3x_7] - d_{10_l}x_{10} \geq 0 \qquad (o)$$

$$-[-133 + 3x_7] + d_{10_u}x_{10} \geq 0 \qquad (p)$$

To solve the alkylation process problem, the code NPSOL, a successive quadratic programming code in MATLAB, was employed.

The values of the objective function found were

$$f(x^0) = 872.3 \text{ initial guess}$$

$$f(x^*) = 1768.75$$

TABLE E14.3B

Deviation parameter	Value
d_{4_l}	99/100
d_{4_u}	100/99
d_{7_l}	99/100
d_{7_u}	100/99
d_{9_l}	9/10
d_{9_u}	10/9
d_{10_l}	99/100
d_{10_u}	100/99

TABLE 14.3C

Variable	Optimal value	Variable	Optimal value
x_1	1698.1	x_6	90.115
x_2	15819	x_7	95.000*
x_3	54.107	x_8	10.493
x_4	3031.2	x_9	1.5618
x_5	2000.0*	x_{10}	153.54

*At bound.

TABLE E14.3D

Constraint	Value at x^*	Constraint	Value at x^*
1(i)	0.33	7(o)	60.9
2(j)	0.18×10^{-11}	8(p)	1.91
3(k)	-0.22×10^{-12}	9(c)	0.29×10^{-10}
4(l)	573	10(d)	0.45×10^{-12}
5(m)	0	11(f)	-0.57×10^{-13}
6(n)	0.45×10^{-12}		

Tables E14.3C and E14.3D list values of the variables at x^* (rounded to five significant figures) and the constraints, respectively, at the optimal solution.

Note that the value of the isobutane makeup x_5 is at its upper bound.

EXAMPLE 14.4 PREDICTING PROTEIN FOLDING

Although the field of molecular modeling is relatively new, it is expanding rapidly with advances in computational power. The appeal of molecular modeling lies in the wealth of potential theoretical developments and practical applications in drug design, food chemistry, genome analysis, and biomedical engineering. A particularly challenging problem involves the prediction of protein folding that can be treated as a global and combinatorial optimization problem. Proteins are three-dimensional structures whose configuration in principal can be predicted from information about a particular amino

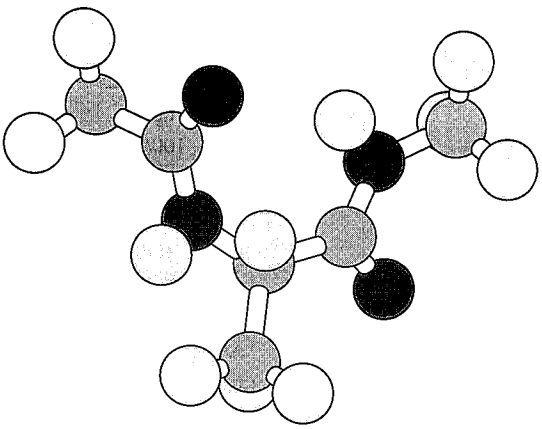

FIGURE E14.4a
Conformation of *N*-acetyl-*N'*-methyl-alanineamide (Courtesy of C. A. Floudas).

acid sequence along with the environmental conditions. Naturally occurring proteins are composed of 20 different amino acid compounds with different side chains and a backbone of repeating units connected by peptide bonds. Covalent bond angles and interatomic forces cause the chain to form and twist in a unique way in three dimensions for each protein. Figure E14.4a illustrates a computer-generated model of the protein *N*-acetyl-*N'*-methyl-alanineamide.

Once the folded sequence is known, the biological and chemical properties of the protein can be predicted. In the development of drugs, for example, the intended target in the human body is a particular protein of known structure whose behavior can be altered (for the better) when a drug molecule binds to a receptor site on the target molecule.

In spite of the complexity of the protein-folding problem, prediction of folding rests on a simple thermodynamic concept: The folded configuration can be identified by minimizing the global free energy of the molecule. Two main components exist, namely the unsolvated potential energy and the solvation energy, the sum of which must be minimized.

$$E \equiv E_{\text{Total}} = E_{\text{Unsol}} + E_{\text{Sol}} \qquad (a)$$

This criterion requires a search through a nonconvex multidimensional conformation space that contains an immense number of minima. Optimization techniques that have been applied to the problem include Monte Carlo methods, simulated annealing, genetic methods, and stochastic search, among others. For reviews of the application of various optimization methods refer to Pardalos et al. (1996), Vasquez et al. (1994), or Schlick et al. (1999).

The example considered here involves the use of a branch-and-bound global optimization algorithm known as αBB (Adjiman et al., 1998) as carried out by Klepeis et al. (1998) who calculated the minimum energy for a number of peptides. To simplify an inherently very complicated optimization problem, particularly in view of the limited data known about solvation parameters, they formulated the energy minimization

problem using the dihedral angles (assuming the covalent bond lengths and bond angles fixed at their equilibrium values) as the optimization variables as follows:

Minimize: $E(\phi_i, \psi_i, \omega_i, \chi_i^k, \theta_j^N, \theta_j^C)$ (*b*)

Subject to:

$$-\pi \le \phi_i \le \pi, \quad i = 1, \ldots, N_{\text{Res}}$$
$$-\pi \le \psi_i \le \pi, \quad i = 1, \ldots, N_{\text{Res}}$$
$$-\pi \le \omega_i \le \pi, \quad i = 1, \ldots, N_{\text{Res}}$$
$$-\pi \le \chi_i^k \le \pi, \quad i = 1, \ldots, N_{\text{Res}}$$
$$k = 1, \ldots, K^i$$
$$-\pi \le \phi_j^N \le \pi, \quad i = 1, \ldots, J_N$$
$$-\pi \le \phi_j^C \le \pi, \quad j = 1, \ldots, J_C$$

where E represents the total of the potential energy function and the free energy of solvation. E_{Unsol} is

$$E_{\text{Unsol}} = \sum_{(ij)\in \text{ES}} \frac{q_i q_j}{r_{ij}} \qquad \text{(Electrostatic contribution-ES)}$$

$$+ \sum_{(ij)\in \text{NB}} F_{ij} \frac{A_{ij}}{r_{ij}^{12}} - \frac{C_{ij}}{r_{ij}^{6}} \qquad \text{(Nonbonded contribution-NB)}$$

$$+ \sum_{(ij)\in \text{HB}} \frac{A'_{ij}}{r_{ij}^{12}} - \frac{B_{ij}}{r_{ij}^{10}} \qquad \text{(Hydrogen bonded contribution-HB)}$$

$$+ \sum_{k\in \text{TOR}} \left(\frac{E_{o,k}}{2}\right)(1 + \cos n_k \theta_k) \qquad \text{(Torsional contribution-TOR)}$$

$$+ \sum_{l\in \text{CL}} 100 \sum_{i=1}^{i=3} (r_{il} - r_{io})^2 \qquad \text{(Cystine loop-closing contribution-CL)}$$

$$+ \sum_{l\in \text{CT}} \left(\frac{E_{o,l}}{2}\right)(1 - \cos n_1 \chi_1) \qquad \text{(Cystine torsional contribution-CT)}$$

$$+ \sum_{p\in \text{PRO}} E_p \qquad \text{(Proline internal contribution-PRO)}$$

where: A_{ij} = nonbonded parameter specific to the atomic pair
A'_{ij} = hydrogen-bonded parameter specific to the atomic pair
B_{ij} = hydrogen-bonded parameter specific to the atomic pair
C_{ij} = nonbonded parameter specific to the atomic pair
$E_{o,k}$ = parameter corresponding to torsional barrier energy for a dihedral angle θ_k
$E_{o,l}$ = parameter corresponding to torsional barrier energy for a dihedral angle χ_l involved in cystine loop closing

E_p = fixed internal energy for each proline residue in the protein
F_{ij} = coefficient equal to 0.5 for one to four interactions and equal to 1.0 for one to five and higher interactions
i = index denoting the sequence of amino acid residues in the peptide chain
j = index denoting the dihedral angles of the amino acid end group
J_C = number of carbolic end groups
J_N = number of dihedral angles of the end group
k = index denoting the dihedral angles of the side chains for the ith amino acid residue
K^i = number of angles on the side chains
N_{Res} = number of amino acid residues
n_k = symmetry type for θ_k
n_l = symmetry type for χ_l
q_i = dipole parameter for atom i
q_j = dipole parameter for atom j
r_{ij} = the interatomic distance in the atomic pair ij
r_{il} = actual interatomic distance
r_{io} = required interatomic distance
$\theta_i, \psi_i, \omega_i$ = dihedral angles along the backbone of the peptide chain
χ_l^k = side chain dihedral angle
θ_j^C = dihedral angles of the carboxy end groups
θ_j^N = dihedral angles of the amino end groups

To reduce undesirable perturbations in the minimization, and for other reasons explained in Klepeis et al., the first term on the right-hand side of Equation (*a*) was minimized before adding the contribution from the second term. The specific details and parameters of problem (*b*) can be found in Klepeis et al.

Klepeis et al. extended the αBB optimization algorithm to guarantee convergence to the global optimum of a nonlinear problem with twice differentiable functions. Without such a guarantee, the outcome depends too heavily on the allocated initial conditions for the molecular configuration. The αBB optimization algorithm brackets the global minimum solution by developing converging lower and upper bounds. These bounds are refined by successively partitioning the region for search. Upper bounds on the global minimum are obtained by local minimizations of the original energy function E. Lower bounds L are obtained by minimizing convex lower-bounding functions that are constructed by adding to E the sum of separable quadratic terms such as

$$\sum_{i=1}^{N_{\text{Res}}} \alpha_{\psi,i}(\psi_i^L - \psi_i)(\psi_i^U - \psi_i)$$

for each angle (6 terms are added).

The α represent nonnegative parameters that must be greater than or equal to the negative one-half of the minimum eigenvalue of the Hessian of E over the defined domain. These parameters can be estimated by the solution of an optimization problem or by using the concept of the measure of a matrix (Maranas and Floudas, 1994). The net result is to make L convex. A useful property of L is that the maximum separation between L and E is bounded and is proportional to α and to the square of the diagonal of the successive box constraints, so that convergence to a global optimum occurs.

At any stage, once solutions for the upper and lower bounds have been established, the next step is to modify the bounding problems for the next iteration. This is accomplished by successively partitioning the initial domain into smaller subdomains. The default partitioning strategy used in the algorithm involves successive subdivision of the original hyper-rectangle by halving on the midpoint of the longest side (bisection). A nonincreasing sequence for the upper bound is found by solving the nonconvex problem E locally and selecting it to be the minimum over all the previously recorded upper bounds.

Initially Klepeis et al. allowed the dihedral angles to vary over the entire $[-\pi, \pi]$ domain. It was found, however, that the problem required intensive computational effort (Androulakis et al., 1997). A reduction of the domain space was therefore proposed by setting limits based on the actual distributions of the dihedral angles. Obviously, for the algorithm to be successful, these reductions could not exclude the region of the global minimum conformation.

The computational requirement of the αBB algorithm depends on the number of variables on which branching occurs. The most important variables are those variables that substantially influence the nonconvexity of the surface and the location of the global minimum. In the protein-folding problem, the backbone dihedral angles (ϕ and ψ) are the most influential variables. Therefore, in very large problems, to further reduce the dimensions of the problem, only these variables were involved in the optimization.

Figure E14.4b shows the results of the application of the optimization strategy to solvated N-acetyl-N'-methyl-alanineamide. Level sets of the deviations of the total energy from the global minimum are shown as solid and dashed lines at 1, 2, 5, and

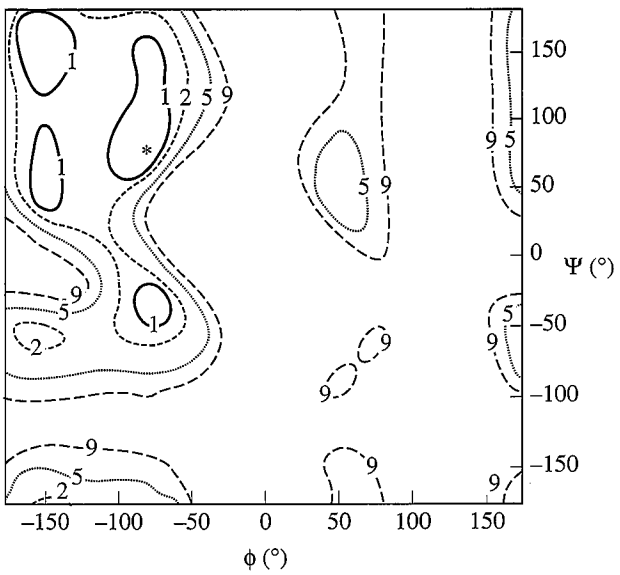

FIGURE E14.4b
Surface of the objective function obtained in determining the structure of N-acetyl-N'-methyl-alanineamide; *is the minimum, and the level sets denote deviations from the minimum (in kcal/mol).

9 kcal/mol, respectively; *designates the global minimum. Klepeis et al. list the various components of the total energy as a function of the amino residues for the protein. Only qualitative comparisons can be made with actual proteins because of the lack of experimental data.

EXAMPLE 14.5 OPTIMIZATION OF LOW-PRESSURE CHEMICAL VAPOR DEPOSITION REACTOR FOR THE DEPOSITION OF THIN FILMS

The manufacture of microelectronic devices involves the sequencing of processes involving thin film deposition, patterning, and doping, only the first of which is discussed here. The formation of the films is performed by a variety of techniques, including physical and chemical processes. One of the most versatile of these methods is chemical vapor deposition (CVD), which involves reacting gases flowing over a wafer to form the desired film. Energy for the reaction is provided by heat or from a plasma. CVD requires the diffusion of gaseous reactants to the hot substrate (wafer), adsorption, reaction, desorption, and diffusion of the gaseous products back into the bulk gas. The net result of the process is formation of a film on the substrate. One common configuration used for CVD stacks the wafers in a tube such as that shown in Figure E14.5a, with heating provided by furnace elements (Middleman and Hochberg, 1993). The low-pressure chemical vapor deposition (LPCVD) reactor allows a large number of wafers to be processed in one batch, yielding good film thickness and composition uniformity.

The LPCVD reactor shown in Figure E14.5a operates at pressures of 0.1–1 torr. The close stacking of the wafers allows for a large throughput while taking advantage of the fact that at these low pressures gas diffusivities are high. This arrangement allows good transport of gases into the region between the wafers (the interwafer region) and hence good radial uniformity of deposition. The flow in the region between the wafer edges and the reactor wall (the annular region) is laminar at typical LPCVD conditions. The reactor walls as well as the wafers are hot so that radial temperature gradients are small. The nonuniformity of growth rates in the radial direction is thus minimized.

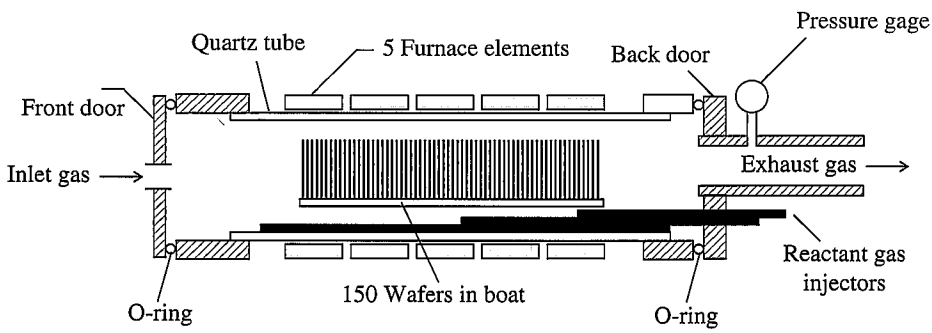

FIGURE E14.5a
A typical multiwafer hot-wall low-pressure chemical vapor deposition reactor.

In most microelectronics fabrication factories ("fabs"), LPCVD of polycrystalline silicon (poly-Si) is carried out by the decomposition silane

$$SiH_4(g) \rightarrow Si(s) + 2H_2(g)$$

The gas-solid reaction rate is modeled by the nonlinear expression

$$R = \frac{k_1 p_{SiH_4}}{1 + k_2 p_{H_2}^{1/2} + k_3 p_{SiH_4}} \qquad (a)$$

where R = the reaction rate
p = the partial pressure
k_1, k_2, k_3 = rate constants

The rate expression is based on adsorption–desorption equilibrium at the substrate surface with an additional term $(k_2 p_{H_2})$ representing H_2 gas inhibition. The rate constants can be estimated by regression of R with the two partial pressures using experimental data (Roenigk and Jensen, 1985).

Model equations. Fundamental process models are very useful in optimizing the design and operation of LPCVD systems. A fundamental model of an LPCVD reactor similar to Figure E14.5a was presented by Jensen and Graves (1983) and included the following simplifying assumptions:

1. The reactor shown in Figure E14.5a, has no radial temperature gradients because its walls and substrate are heated and slow reaction rates imply small heats of reaction.
2. The axial temperature gradient is fixed by the furnace settings because the gas heat-up lengths are small and most heat transfer occurs by radiation at LPCVD conditions.
3. There is no axial variation of gas-phase composition in the interwafer region between any two consecutive wafers because the interwafer spacing is small.
4 There is no radial variation of gas-phase composition in the annular region because the annular region is small, and because there is rapid diffusion at LPCVD conditions.
5. The gas phase is in steady state, because CVD growth processes are slow compared to gas phase dynamics.

These five assumptions were used by Jensen and Graves (1983) and were also employed in the design study of Setalvad and colleagues (1989). Define N_r and N_z as the molar respective fluxes of silane in the r and z directions, Δ as the interwafer spacing, and x_1 as the mole fraction of silane in the gas phase. The mass transport equations in the r and z directions that describe the diffusion of silane consist of two coupled partial differential equations. In Setalvad and colleagues (1989), the partial differential equations in the r and z directions were converted to ordinary differential equations by assuming the axial transport (N_z) only occurred in the annular region, whereas the radial transport (N_r) only occurred in the interwafer region (see Figure E14.5b). The LPCVD model thus is as follows.

Interwafer Region

$$\frac{\Delta}{r}\frac{d}{dr}(rN_{r1}) = -2R \qquad (b)$$

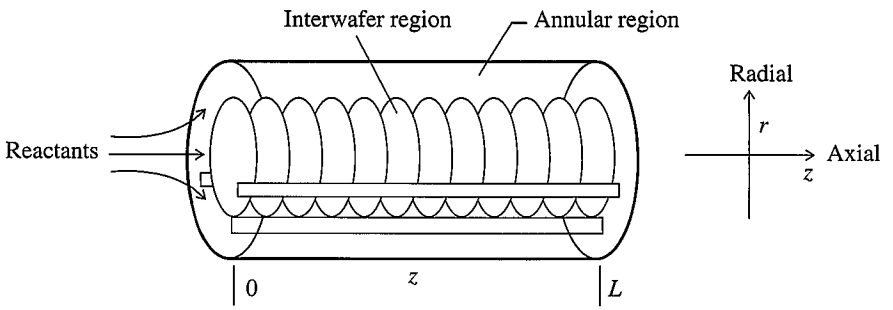

FIGURE E14.5b
LPCVD reactor geometry with interwafer and annular regions.

with boundary condition:

$$\left.\frac{dx_1}{dr}\right|_{r=0} = 0 \quad \text{and} \quad x_1(r_w^-) = (r_w^+) \tag{c}$$

where r_w = the wafer radius, and
+,− refers to an infinitesimal distance in postive/negative r direction

Annular Region

$$\frac{dN_{z_1}}{dz} = -\frac{2R}{(r_t^2 - r_w^2)}\left[r_t(1 + a) + \frac{r_w^2}{\Delta}\eta\right] \tag{d}$$

where r_t = the tube radius
a = the area of the wafer holder plus wafers relative to the reactor tube area

The fluxes are related to the mole fraction through Fick's law (c is total concentration of gas, and D is the diffusivity of the silane in the gas phase):

$$N_{r_1} = cD\frac{dx_1}{dr} \tag{e}$$

$$N_{z_1} = cD\frac{dx_1}{dz} \tag{f}$$

Boundary conditions for the annular region are given at the inlet ($z = 0$) and the tube exit ($z = L$):

$$\left.N_{z_1}\right|_{z=0} = v_0 c_0 x_{10} \quad \text{and} \quad \left.\frac{dx_1}{dz}\right|_{z=L} = 0 \tag{g}$$

where $v_0 c_0 x_{10}$ represents the product of gas velocity, total concentration, and mole fraction silane at the inlet.

The effectiveness factor η is defined as

$$\eta = \frac{2\int_0^{r_w} rR(r)dr}{r_w^2 R\Big|_{r_w}} \tag{h}$$

η is the ratio of the average rate of deposition on a wafer to that at its edge, so it is a measure of the uniformity of deposition. The rate R at r_w varies in the z direction, hence η is a function of axial distance z. The effectiveness factor represents the radial uniformity of deposition. When surface reaction is rate-controlling, $\eta = 1$, and when $\eta < 1$, diffusion resistance comes into play.

Optimization of the reactor. The nonlinear ordinary differential equations and boundary conditions in the model can be put in dimensionless form and converted to algebraic equations using orthogonal collocation (Finlayson, 1980). Setalvad and coworkers (1989) used these algebraic equations as constraints in formulating a nonlinear programming problem to study the effects of temperature, flow parameters, reactor geometry, and wafer size on the LPCVD process, particularly the uniformity of silicon deposition. Strategies were devised to determine the potential improvements in the system performance by using optimum temperature staging and reactant injection schemes. Figure E14.5c shows the inputs and performance measures for the reactor that can be optimized to maximize the film growth rate (production rate), subject to constraints on radial film uniformity (on each wafer), as well as axial uniformity (wafer-to-wafer).

The growth rate is quite sensitive to the axial temperature profile. An axial temperature profile that increases along the reactor because it improves the deposition uniformity is commonly used in industry. The temperature of each successive zone in the furnace (defined by the furnace elements in Figure E14.5a) can be adjusted by voltage applied to variac heaters. The zone temperatures are assumed constant within each zone, $T_j, j = 1, \ldots, n_{tz}$, where n_{tz} is the number of temperature zones to be used,

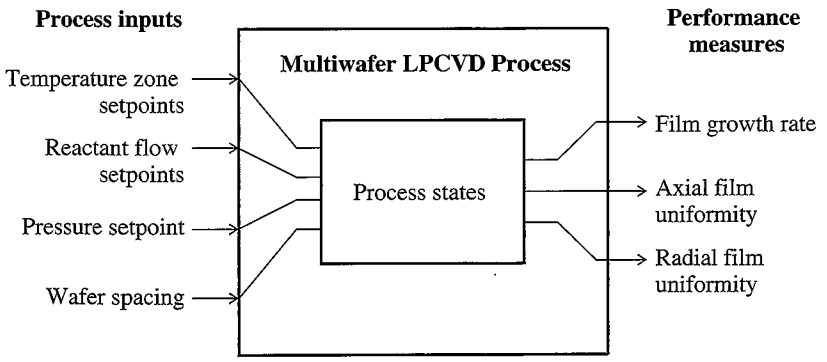

FIGURE E14.5c
Multiwafer LPCVD reactor process inputs and outputs.

typically three to five. The optimization procedure was initiated with all T_j values equal to 880 K. The objective function to be maximized in this case was

$$f(\mathbf{T}) = \int_0^L [G(\mathbf{T}, z)]^2 dz \cong \sum_{i=1}^{N} [G_i(\mathbf{T}, z)]^2 \Delta z_i \qquad (i)$$

G_i is determined by averaging the growth rate given by Equation (*a*) over the wafer surface, which is then integrated over the axial direction to compute $f(\mathbf{T})$. G is measured in Å/min, $\mathbf{T}$ is the set of temperatures, and z_i ($i = 1, N$) are locations along the reactor at which the model is solved to obtain the rates G_i. $f(\mathbf{T})$ is a uniformly weighted sum of the deposition rates over the entire reactor (N = number of increments) obtained via the LPCVD model, thus representing the throughput of the reactor.

The objective function is maximized subject to the following inequality constraints:

1. The maximum allowable axial variation in growth rate is 5% of the maximum rate,

$$V = \frac{\max(G_i) - \min(G_i)}{\max(G_i)} \leq 0.05 \qquad (j)$$

2. At no point should the radial variation in growth rate be greater than 5%; in terms of effectiveness factors,

$$\eta_i \geq 0.95, \quad i = 1, \ldots, n_{tz} \qquad (k)$$

3. The temperature in each zone is restricted to

$$880 \text{ K} \leq T_i \leq 890 \text{ K}, \quad i = 1, \ldots, n_{tz} \qquad (l)$$

This last constraint is imposed so that the grain size and other temperature-dependent material properties of the grown film and also its step coverage do not show excessive variations.

The nonlinear programming problem based on objective function (*i*), model equations (*b*)–(*g*), and inequality constraints (*j*)–(*l*) was solved using the generalized reduced gradient method presented in Chapter 8. See Setalvad and coworkers (1989) for details on the parameter values used in the optimization calculations, the results of which are presented here.

In Figure E14.5d the performance of the reactor with operation with each of three temperature zones at their optimal values can be compared with the isothermal case (T_i = 880 K). The optimization routine increased the temperature of zone 3 the most, followed by zone 2 (see Figure E14.5e). The optimization strategy increased the value of $f(\mathbf{T})$ while decreasing the maximum axial growth rate variation. The temperatures were increased from the initial value (880 K) until the axial rate variation (m_i) between the beginning and the end of zone 3 reached the 5% limit. Reactant depletion causes the sharp drop-off in rate within the zone. This effect of reactant depletion increases noticeably from zone 1 to zone 3 (Figure E14.5d). The temperature in zone 2 could be decreased so that less reactant is consumed in this zone and more is available for zone 3. However, the resulting lower rates in zone 2 cause the axial rate variation between the end of this zone and the beginning of zone 3 to exceed the 5% limit.

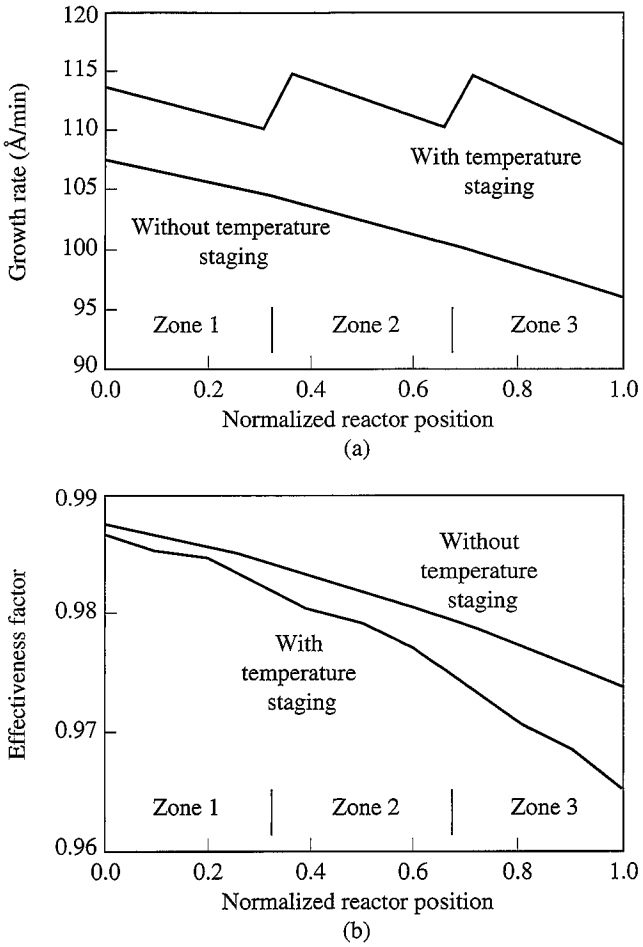

FIGURE E14.5d
Reactor performance with and without optimized temperature staging.

Optimum reactant injection. An alternative to using temperature staging is to provide a sudden increase in the partial pressure of SiH_4, using the reactant gas injectors shown in Figure E14.5a, so that additional reactant is fed into the reactor at different points along its length. Sudden increases in growth rate at the injection points result without the disadvantage of excessive rate drop-off due to reactant depletion, as seen for the case of temperature staging. For modeling purposes the original reactor with two reactant injection ports can be considered to consist of three smaller reactors or subreactors. Predicting the performance of the reactor then involves consecutively solving the modeling equations for each of the subreactors; see Setalvad and coworkers (1989) for more details.

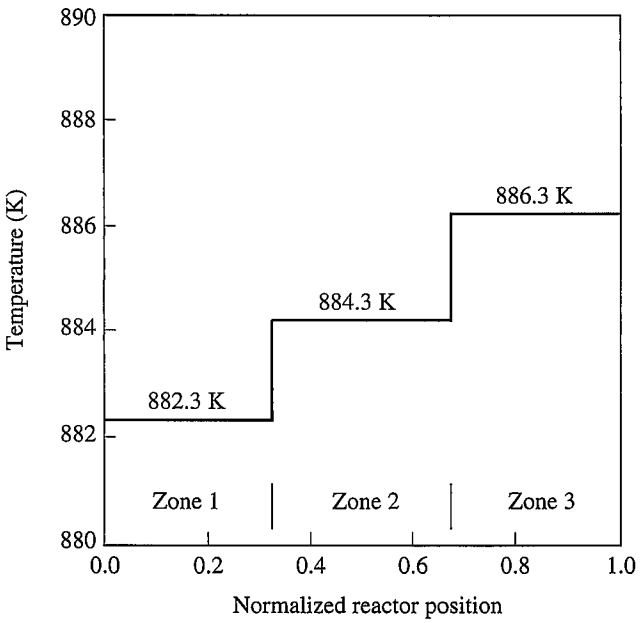

FIGURE E14.5e
The optimum temperature profile for three stages.

The optimization problem for the case of sudden injection of SiH_4 involves as independent variables the total gas flow velocities:

$$v_{0i}, \quad i = 1, \ldots, n_{\text{inj}}$$

based on the total amount of gas injected, and

$$x_{1i}, \quad i = 1, \ldots, n_{\text{inj}}$$

the mole fractions of the reactant silane in each injection stream. Here n_{inj} is the number of injection points. Two intermediate injection points were considered, giving four independent variables to be adjusted (two velocities and two mole fractions). This formulation was thought to be a reasonable balance between improved reactor performance and the resulting greater design complexity.

The objective function to be maximized was essentially the same as before except that the rate G was now a function of v_{oi} and x_{li} instead of T_i, that is,

$$f(\mathbf{v}_0, \mathbf{x}_1) = \int_0^L G[(\mathbf{v}_0, \mathbf{x}_1, z)]^2 \, dz \approx \sum_{i=1}^{N} [G_i(\mathbf{v}_0, \mathbf{x}_{1i}, z_i)]^2 \Delta z_j \qquad (m)$$

The uniformity inequality constraints [Equations (j)–(l)] were again included in the problem. Additionally, the bounds on the variables were

$$0.0 \leq x_{1i} \leq 1.0, \quad i = 1, \ldots, n_{\text{inj}} \qquad (n)$$

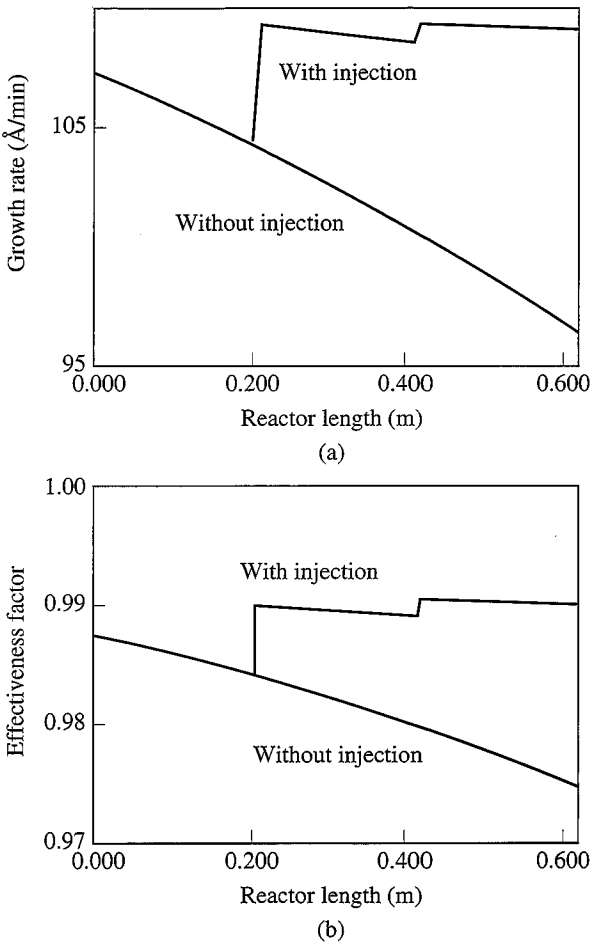

FIGURE E14.5f
Reactor performance with optimum staged injection.

and

$$0.03 \leq v_{0i} \leq 0.5, \quad i = 1, \ldots, n_{\text{inj}} \tag{o}$$

The optimum reactor growth rate and effectiveness factor are shown in Figure E14.5f. As expected, the optimization code adjusted v_{01} first because the deposition was more sensitive to flow velocities. After v_{01} reached its upper bound, x_{11} increased until the axial uniformity constraint was reached, that is, the difference in growth rate between the end of the first zone and the beginning of the second was equal to 5% of the inlet value (see Figure E14.5f) according to constraint (j). However, for injection point 2, the rates did not change by 5% between the injection points. Maximizing overall growth rate was more easily solved by increasing x_{12}. The effectiveness factors (Figure E14.5f), unlike those in the previous temperature profile optimization (Figure E14.5d) stayed nearly constant along the axial direction.

Setalvad and coworkers (1989) also evaluated nonuniform interwafer spacing in the reactor to improve deposition uniformity and increase the reactor throughput. Optimal interwafer spacings were smaller toward the reactant inlet to take advantage of the larger reactant concentration in this region, and larger at the end of the reactor where reactant depletion and hydrogen production inhibited the polysilicon deposition. This scheme exhibited decreased sensitivity of the process to gas flow rate variations when compared with the uniformly spaced wafer case.

A subsequent study by Badgwell and colleagues (1992) used a more detailed deposition model that was verified on industrial-scale LPCVD equipment. Badgwell and colleagues showed a sharp decrease in deposition uniformities for a wafer to reactor diameter ratio of about 0.5. This outcome suggested that it may not be wise to use existing reactors for larger wafer sizes. Furthermore, the reactor tubes that would then be necessary may have to be inordinately large and, in view of the low pressures, inordinately thick to be economical.

EXAMPLE 14.6 REACTION SYNTHESIS VIA MINLP

Process synthesis involves intelligent decision making to select a process design whose configuration and operating states are optimal in some sense. The development of mixed-integer nonlinear programming (MINLP) algorithms has greatly expanded the scope of quantitative synthesis because we can now treat synthesis problems involving both continuous and discrete variables. In this example, we demonstrate the use of MINLP in the synthesis of a hydrodealkylation (HDA) process (Douglas, 1988) as carried out by Phimister and colleagues (1999).

The fundamental decisions in the synthesis of a multistep process that involves individual reactor units connected in serial and parallel configurations as well as recycle pertain to how the units will be connected. In addition, however, we must consider (for a steady-state process)

1. What the feeds and their quantities should be.
2. What reaction paths to avoid.
3. What products should be made and in what quantity.
4. What the flow rates should be.
5. What variables affect the products.
6. How to maintain flexibility.
7. Safety issues.

We consider only factors 1 through 4 in what follows. Phimister and colleagues decomposed the strategy of reactor process design so that a mathematical statement of the synthesis problem could be formulated in terms of an objective function and constraints. At the initial stage of the decision making, the designer is presumed to have limited information about possible reaction paths as reflected in kinetic models, costs of raw materials, selling prices of products, and the desired plant production. The MINLP problem formulation in this example includes (1) binary decision variables designating whether or not a connection exists between reactors, (2) specification of continuous variables corresponding to flow rates, and (3) prespecification of the extent of conversion of a reactant.

From the topographical viewpoint illustrated in Figure E14.6a the process comprises a set of reactor–separator sections that connect a set of component feeds (specified as source nodes) to component products (specified as destination nodes). Each section is a prescribed sequence of reactors and associated separation units, and sev-

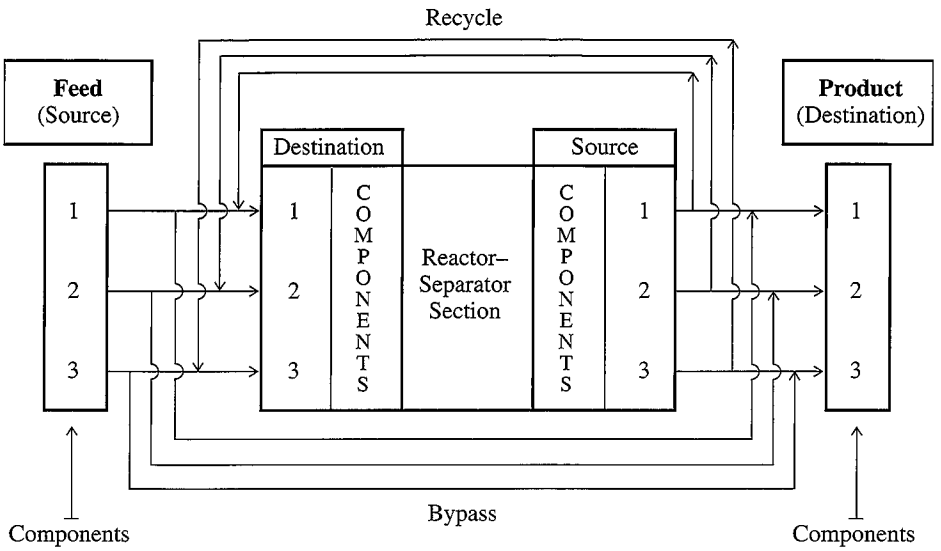

FIGURE E14.6a
Schematic of reactor–separation process.

eral sections may be interconnected, although for simplicity in presentation, we show only one such section in this example. The details of the design of the reactors and separators constituting a section are determined after the MILNP problem is solved. A source node defines the site from which a component is supplied, and a destination node defines the site at which a component is required in the process. In the initial topography (see Figure E14.6a) for the process, all of the components in the nodes are connected via directed paths, except that usually no feedback exists from a process component destination to a process component source. By use of binary variables in the constraints (as we will show later), a set of paths can be eliminated from the MINLP problem formulation, thus simplifying the topography. Various connections may be required, such as a particular feed from an external source node to a section, and various connections may be deleted, such as a bypass path from a process source to a process destination or a recycle path for a section.

The notation used in this example for the connections is as follows:

D = the set of destination nodes $\{1, 2, \ldots, e\}$ including reactor–separator sections (recycle) or flows exiting the overall process
e = the process exit stream
f = the process feed stream
n = the number of components
N = the total number of plant reactor–separator sections
Q = the set of components, $i = 1, 2, \ldots n$
S = the set of source nodes $\{f, 1, 2, \ldots, N\}$
X = fraction conversion of toluene
$y_{i,j,k}$ = a binary variable (0, 1) in which the subscript i designates the chemical component, j denotes the source node, and k denotes the destination node
ψ = selectivity of toluene converted to benzene

As examples of the notation for the binary variables, $y_{CH_4,f,2} = 1$ means that methane in the feed stream goes to the reactor–separator section labeled No. 2, $y_{H_2,f,e} = 0$ means that hydrogen in the feed stream does not go directly to the exit stream, and $y_{CO,1,1}$ means that carbon monoxide is recycled in the reactor–separator section labeled No. 1.

Stream flow rates F that exit are designated with the same set of subscript indices, i, j, and k, that have the same meaning as that used for the binary variables. Negative flow rates are not allowed ($F_{i,j,k} \geq 0$). Constraints such as

$$F_{i,j,k} - Uy_{i,j,k} \leq 0$$

where U is the largest flow rate allowed between two sites, place an upper bound on a flow rate.

The reaction(s) in a reactor–separator section is accounted for by an equality constraint(s) such as for the case of $A \rightarrow B$ in section 1

$$\sum_k F_{A,1,k} = (1 - X) \sum_j F_{A,j,1}$$

$$\sum_k F_{B,1,k} = \sum_j F_{B,j,1} + X \sum_j F_{A,j,1}, \quad j \in S, k \in D$$

where X is the fraction conversion of A to B.

In the HDA process represented in Figure E14.6.b (Douglas (1988), the reactions are

$$\underset{\text{Toluene}}{C_7H_8} + \underset{\text{Hydrogen}}{H_2} \rightarrow \underset{\text{Benzene}}{C_6H_6} + \underset{\text{Methane}}{CH_4}$$

$$\underset{\text{Benzene}}{C_6H_6} \leftrightarrow \underset{\text{Diphenyl}}{C_{12}H_{10}} + \underset{\text{Hydrogen}}{H_2}$$

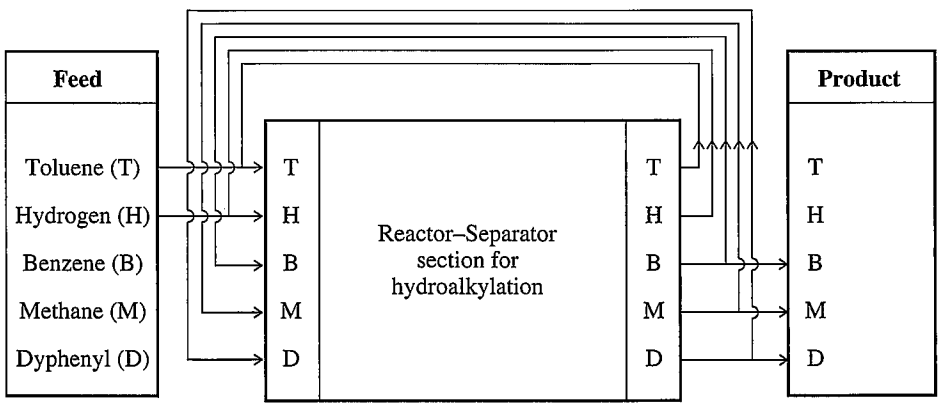

FIGURE E14.6b
Component flow diagram.

From Figure E14.6b you can see that five components exist for the one reactor–separator section, and 20 binary variables and stream flows (continuous variables) occur in the initial model. Let us summarize the model proposed by Phimister and colleagues. Other details are in Douglas.

Constraints Involving Binary Variables

Bypass prohibited:

$$\sum_i y_{i,f,e} = 0, \quad i \in Q \tag{a}$$

Only toluene and hydrogen are feeds:

$$y_{C_6H_6,f,1} + y_{C_{12}H_{10},f,1} + y_{CH_4,f,1} = 0 \tag{b}$$

$$y_{C_7H_8,f,1} = 1 \tag{c}$$

$$y_{H_2,f,1} = 1 \tag{d}$$

Only benzene, methane, and diphenyl leave the process

$$y_{C_6H_6,1,e} = 1 \tag{e}$$

$$y_{CH_4,1,e} = 1 \tag{f}$$

$$y_{C_{12}H_{10},1,e} = 1 \tag{g}$$

No toluene exits the process to a destination

$$\sum_j y_{C_7H_8,j,e} = 0 \tag{h}$$

For the reactor–separator section, all source nodes must have a destination

$$\sum_k y_{i,1,k} \geq 1, \quad k \in D, \quad \forall i \tag{i}$$

Constraints Representing the Model

Douglas (1988, Appendix B) fit the selectivity of the data ψ versus X given in the 1967 AIChE Student Contest Problem to get

$$\psi = \frac{\text{Moles benzene formed}}{\text{Moles toluene converted}} = 1 - \frac{0.0036}{(1 - X)^{1.544}} \tag{j}$$

$$X \leq 0.97 \tag{k}$$

$$0.20 \leq \psi \leq 1.0 \tag{l}$$

Process Specifications

Production of benzene

80,000 metric ton per year (8000 = hour operation)

Molar feed

$$\frac{\text{Hydrogen}}{\text{Toluene}} = \frac{5 \text{ mol}}{1 \text{ mol}} \qquad (m)$$

Objective Function

The objective function is to maximize profits, namely, products sold minus raw material costs. No capital or investment cost are involved in this example.

To prevent internal flow rates having zero shadow costs at the solution and therefore to avoid a multiplicity of solutions, a penalty of 0.05 times the price is incurred for each ton transported between a source and a destination.

Prices and Costs for Components

Component	Price/cost ($/ton)
Toluene	200
Hydrogen	100
Benzene	500
Methane	100
Diphenyl	20

Phimister and colleagues obtained the optimal configuration and associated flow rates shown in Figure E14.6c using GAMS. The optimal value of the conversion was 0.697, and the selectivity ψ was 0.977, yielding a value of the objective function of $18.65 million/year. Refer to Phimister and colleagues (1999) for a problem corresponding to a more complex plant involving four reactor–separator units and ten components.

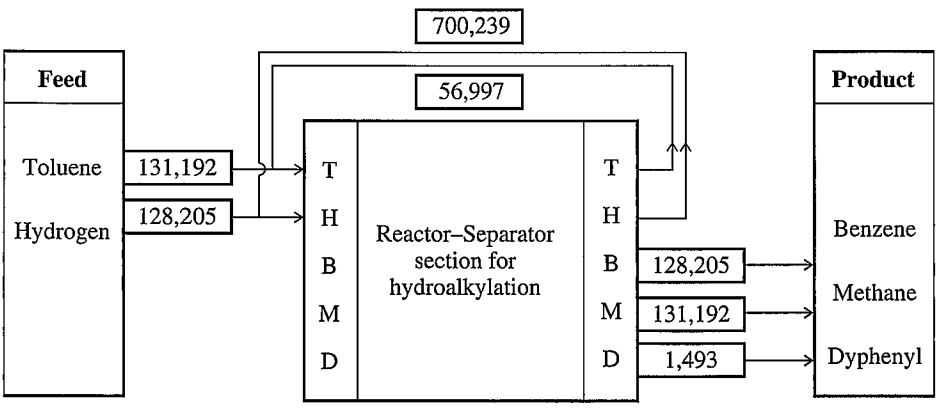

FIGURE E14.6c
Optimal configuration and stream flows.

REFERENCES

Adjiman, C. S.; I. P. Androulakis; and C. A. Floudas. "A Global Optimization Method, αBB for General Twice-Differentiable NLPs—II. Implementation and Computational Results." *Comput Chem Eng* **22:** 1159–1179 (1998).

Androulakis, I. P.; G. D. Maranas; and C. A. Floudas. "Global Minimum Potential Energy Conformation of Oligo Peptides." *J Glob Opt* **11:** 1–34 (1997).

Badgwell, T. A.; I. Trachtenberg; and T. F. Edgar. "Modeling and Scale-Up of Multiwafer LPCVD Reactors." *AIChE J* **38**(6): 926–938 (1992).

Douglas, J. M. *Conceptual Design of Chemical Processes*. McGraw-Hill, New York (1988).

Finlayson, B. *Nonlinear Analysis in Chemical Engineering*. McGraw-Hill, New York, 1980.

Fogler, H. S. *Elements of Chemical Reaction Engineering*. Prentice-Hall, Upper Saddle River, NJ (1998).

Froment, G. F.; and K. B. Bischoff. *Chemical Reactor Analysis and Design*. Wiley, New York (1990).

Jensen, K. F.; and D. B. Graves. "Modeling and Analysis of Low Pressure CVD Reactors." *J Electrochem Soc* **130:** 1950–1957 (1983).

Klepeis, J. L.; I. P. Androulakis; M. G. Ierapetritou, et al. "Predicting Solvated Peptide Configuration via Global Minimization of Energetic Atom-to-Atom Interactions." *Comput Chem Eng* **22:** 765–788 (1998).

Levenspiel, O. *Chemical Reaction Engineering*. Wiley, New York (1998).

Maranas, C. D.; and C. A. Floudas. "A Deterministic Global Optimization Approach for Molecular Structure Determination." *J Chem Phys* **100:** 1247–1261 (1994).

Middleman, S.; and A. K. Hochberg. *Process Engineering Analysis in Semiconductor Device Fabrication*. McGraw-Hill, New York, 1993.

Missen, R. W.; C. A. Mims; and B. A. Saville. *Introduction to Chemical Reaction Engineering and Kinetics*. Wiley, New York (1998).

Murase, A.; H. L. Roberts; and A. O. Converse. "Optimal Thermal Design of an Autothermal Ammonia Synthesis Reactor." *Ind Eng Chem Process Des Dev* **9:** 503–513 (1970).

Pardalos, P. M.; D. Shalloway; and G. Xue (editors). "Global Minimization of Nonconvex Energy Functions, Molecular Conformation and Protein Folding." DIMACS Series in Discrete Mathematics and Theoretical Computer Science, **23,** American Mathematical Society, Providence, RI (1996).

Phimister, J. R.; E. S. Fragar; and J. W. Ponton. "The Synthesis of Multistep Process Plant Configurations." *Comput Chem Eng* **23:** 315–326 (1999).

Roenigk, K. F; and Jensen, K. F. "Analysis of Multicomponent LPCVD Processes." *J Electrochem Soc* **132:** 448–455 (1985).

Sauer, R. N.; A. R. Coville; and C. W. Burwick. "Computer Points Way to More Profits." *Hydrocarbon Process Petrol* Ref. **43:** 84–92 (1964).

Schlick, T.; R. D. Skeel; A. T. Brunger, et al. "Algorithmic Challenges in Computational Molecular Biophysics." *J Comput Phys* **151:** 9–48 (1999).

Schmidt, L. D. *The Engineering of Chemical Reactions*. Oxford Univ. Press, Oxford (1997).

Setalvad, T.; I. Trachtenberg; B. W. Bequette, et al. "Optimization of a Low Pressure CVD Reactor for the Deposition of Thin Films." *IEC Res* **28:** 1162–1172 (1989).

Vasquez, M.; G. Nemethy; and H. A. Scheraga. "Conformational Energy Calculations of Polypeptides and Proteins." *Chem Rev* **94:** 2183–2239 (1994).

SUPPLEMENTARY REFERENCES

Abel, O.; A. Helbig; W. Marquardt; H. Zwick, et al. "Productivity Optimization of an Industrial Semi-batch Polymerization Reactor Under Safety Constraints." *J Proc Contr* **10:** 351–362 (2000).

Balakrishna, S.; and L. T. Biegler. "Targeting Strategies for the Synthesis and Energy Integration of Nonisothermal Reactor Networks." *Ind Eng Chem Res* **31:** 2152–2164 (1992).

Bonvin, D. "Optimal Operation of Batch Reactors—A Personal View." *J Proc Contr* **8:** 355–368 (1998).

Edwards, K.; V. Manousiouthakis; and T. F. Edgar. "Kinetic Model Reduction Using Genetic Algorithms." *Comput Chem Eng* **22:** 239–246 (1998).

Feinberg, M.; and D. Hildebrandt. "Optimal Reactor Design from a Geometric Viewpoint: I. Universal Properties of the Attainable Region." *Chem Eng Sci* **52**(10): 1637–1666 (1997).

Geddes, D.; and T. Kubera. "Integration of Planning and Real-Time Optimization Olefins Production." *Comput Chem Eng* **24:** 1645–1649 (2000).

Guntern, C.; A. H. Keller; and K. Hungerbühler. "Economic Optimization of an Industrial Semi-batch Reactor Applying Dynamic Programming." *Ind Eng Chem Res* **37**(10): 4017–4022 (1998).

Hildebrandt, D.; and L. T. Biegler. "Synthesis of Reactor Networks." In *Foundations of Computer Aided Process Design '94, AIChE Symposium Series.* L. T. Biegler; M. F. Doherty eds. **91:** 52–68 (1995).

Kokossis, A. C.; and C. A. Floudas. "Optimization of Complex Reactor Networks—I. Isothermal Operation." *Chem Eng Sci* **45**(3): 595–614 (1990).

Lakshmanan, A.; and L. T. Biegler. "Synthesis of Optimal Reactor Networks." *Ind Eng Chem Res* **35**(4): 1344–1353 (1996).

Luus, R. "Optimization of Fed-batch Fermentors by Iterative Dynamic Programming. *Biotechnol Bioeng* **41:** 599–602 (1992).

Rajesh, J. K.; S. K. Gupta; G. P. Rangaiah; and A. K. Ray. "Multiobjective Optimization of Steam Reformer Performance Using Genetic Algorithm." *Ind Eng Chem Res* **39**(3): 706–717 (2000).

Schweiger, C. A.; and C. A. Floudas. "Optimization Framework for the Synthesis of Chemical Reactor Networks." *Ind Eng Chem Res* **38**(3): 744–766 (1999).